Surface instability and chemical reactivity of ZrSiS and ZrSiSe nodal-line semimetals

Danil W. Boukhvalov[1,2,*], Raju Edla[3], Anna Cupolillo[4], Vito Fabio[4], Raman Sankar[5,6], Yanglin Zhu[7], Zhiqiang Mao[7], Jin Hu[8], Piero Torelli[3], Gennaro Chiarello[4,*], Luca Ottaviano[9] and Antonio Politano[9,*]

[1]*College of Science, Institute of Materials Physics and Chemistry, Nanjing Forestry University, Nanjing 210037, P. R. China*
[2] *Theoretical Physics and Applied Mathematics Department, Ural Federal University, Mira Street 19, 620002 Ekaterinburg, Russia*
[3] *Consiglio Nazionale delle Ricerche (CNR)- Istituto Officina dei Materiali (IOM), Laboratorio TASC in Area Science Park S.S. 14 km 163.5 34149 Trieste, Italy*
[4] *Dipartimento di Fisica, Università della Calabria, via ponte Bucci cubo 31/C, 87036 Rende, Cosenza, Italy*
5 Institute of Physics, Academia Sinica, Nankang, Taipei 11529, Taiwan
6 Center for Condensed Matter Sciences, National Taiwan University, Taipei 10617, Taiwan
7 Department of Physics, Pennsylvania State University, 104 Davey Lab University Park, PA 16802-6300
8 Department of Physics, Institute for Nanoscience and Engineering, University of Arkansas, Fayetteville, AR 72701, USA
9 Dipartimento di Scienze Fisiche e Chimiche (DSFC), Università dell'Aquila, Via Vetoio 10, I-67100 L'Aquila, Italy

ABSTRACT
Materials exhibiting nodal-line fermions promise superb impact on technology for the prospect of dissipationless spintronic devices. Among nodal-line semimetals, the ZrSiX (X=S, Se, Te) class is the most suitable candidate for such applications. However, surface chemical reactivity of ZrSiS and ZrSiSe has not been explored yet. Here, by combining different surface-science tools and density functional theory, we demonstrate that the formation of ZrSiS and ZrSiSe surfaces by cleavage is accompanied by the washing up of the exotic topological bands giving rise to the nodal line. Moreover, while the ZrSiS has a termination layer with both Zr and S atoms, in the ZrSiSe a reconstruction occurs with the appearance of Si surface atoms, particularly prone to oxidation. We demonstrate that the chemical activity of ZrSiX compounds is mostly determined by the interaction of Si layer with the ZrX sublayer. A suitable encapsulation for ZrSiX should not only preserve their surfaces from interaction with ox-

This is the author manuscript accepted for publication and has undergone full peer review but has not been through the copyediting, typesetting, pagination and proofreading process, which may lead to differences between this version and the Version of Record. Please cite this article as doi: 10.1002/adfm.201900438.

idative species, but also provide a saturation of dangling bonds with minimal distortion of the surface.

Corresponding authors
*danil@njfu.edu.cn (Prof. Danil W. Boukhvalov)
*gennaro.chiarello@fis.unical.it (Prof. Gennaro Chiarello)
*antonio.politano@univaq.it (Prof. Antonio Politano)

Introduction

After the advent of topological quantum matter [1-7], topological semimetals have triggered the interest of the scientific community for the presence of topologically protected Dirac-like quasiparticles in their bulk [3, 5, 8-10]. This peculiarity makes them particularly appealing for technological exploitation. Conversely, other Dirac materials such as graphene[11-14] and borophene [15-18] require the implementation of a single layer, which remains challenging for industrial applications. Among topological semimetals, in nodal-line semimetals (NLSM) conduction and valence bands cross each other[19, 20]. In particular, in NLSM topological constraints protect band crossings and, moreover, band touching form nodal lines or rings [21]. Recently, topological nodal lines have been observed in bulk ZrSiX compounds [21-25] (X=S, Se, Te). In ZrSiX, a tetragonal structure is formed by the stacking of X-Zr-Si-Zr-X slabs covalently bonded between each other, whose strength decreases by replacing S with Se or Te ions, due to the increase of the ionic radius [26]. This class of materials exhibits large and non-saturating magnetoresistance [27] and ultrahigh mobility of charge carriers (as high as $3 \cdot 10^4$ $cm^2V^{-1}s^{-1}$ at T=3 K [28]).

However, two crucial experimental bottlenecks have to be overcome in order to succeed in technology transfer: (i) the achievement of single crystals with excellent crystalline quality; (ii) the control over surface phenomena, including oxidation, degradation and surface reconstruction. Only recently, our groups have improved the synthesis of bulk single crystals of ZrSiS [28] and ZrSiSe [22], also using only non-toxic and Earth-abundant elements. Neverthe-

less, though previously ZrSiS has been just assumed to be very stable even in air[29-31], a careful investigation on ambient stability of ZrSiX is missing yet.

Moreover, surface properties are completely unknown. The presence of dangling bonds at the surface arising from the truncation of the crystal may originate unexpected surface reconstructions or surface states. As an example, the surface of Bi_2Se_3 topological insulator can reconstruct with Bi bilayers[32], while in NbAs and TaAs Weyl semimetals dangling bonds form Fermi-arc surface states[33]. Furthermore, it remains unclear how the topological properties could be connected to their chemical stability, expressly at the surface. Hence, the energetics of adsorption of reactants at sites located at the surface and eventual surface reconstructions should be evaluated in order to unveil the chemical stability and, correspondingly, the catalytic properties of NLSM samples.

Here, we combine surface-science techniques with density functional theory (DFT) to unveil the peculiarities and the chemical reactivity of surfaces of ZrSiS and ZrSiSe. We find that the formation of the surface implies the removal of topological properties. Furthermore, while ZrSiS exhibits a termination with both Zr and S atoms, the ZrSiSe surface reconstructs with the appearance of surface Si atoms particularly prone to oxidation. We show that the chemical activity of ZrSiX compounds is largely determined by the interaction of Si layer with the ZrX sublayer and, accordingly, we clarify the features of encapsulation procedures required to successfully exploit ZrSiX in technology.

Results and Discussion

The outstanding crystalline quality of these samples is ensured by the sharp (00*n*) features in their X-ray diffraction (XRD) patterns [22, 28] and by the exceptionally flatness of their surfaces (see Fig. S1 in the Supporting Information, SI). The presence of peculiar topological prop-

erties as NLSM of our single crystals has been previously demonstrated by magnetotransport data for ZrSiS [28] and ZrSiSe [22].

Vibrational spectroscopy is a powerful tool to monitor modifications in surface chemical bonds [34]. Especially, high-resolution electron energy loss spectroscopy (HREELS) is sensitive to the outermost surface layer. Figure 1 shows the vibrational spectra of pristine and defected ZrSiS exposed to a dose of 10^3 L (1 L=10^{-6} torr·s) of O_2 at room temperature. The pristine ZrSiS has a featureless vibrational spectrum, due to the absence of any contamination on as-cleaved samples. The pristine, undefected surface is also quite inert toward oxygen, as indicated by the analysis of the corresponding vibrational spectrum of the O_2-dosed undefected ZrSiS. Therefore, one can estimate the sticking coefficient of oxygen to be less than 10^{-3} at room temperature. We obtained surface oxidation only for ZrSiS with a considerable amount of defects, introduced by ion sputtering. The bombardment with argon ions selectively removes Si and S compared to Zr, due to the very dissimilar atomic masses. The O_2-dosed surface with modified surface stoichiometry ($Zr_{1.05}Si_{0.98}S_{0.97}$) has an excitation spectrum dominated by an intense peak at 83 meV, with its corresponding replica at 166 meV. The strong intensity of the feature at 83 meV (as high as 15% of the elastic peak) is typical of Fuchs-Kliewer phonons[35]. We have compared the experimental loss spectrum with the excitation spectrum of optical phonons of bulk ZrO_2 in literature [36], finding good overlap with only a slight deviation in phonon energies (Fig. S2 in the SI). We note the absence of vibrations connected to Si-O bonds (see below discussion for ZrSiSe).

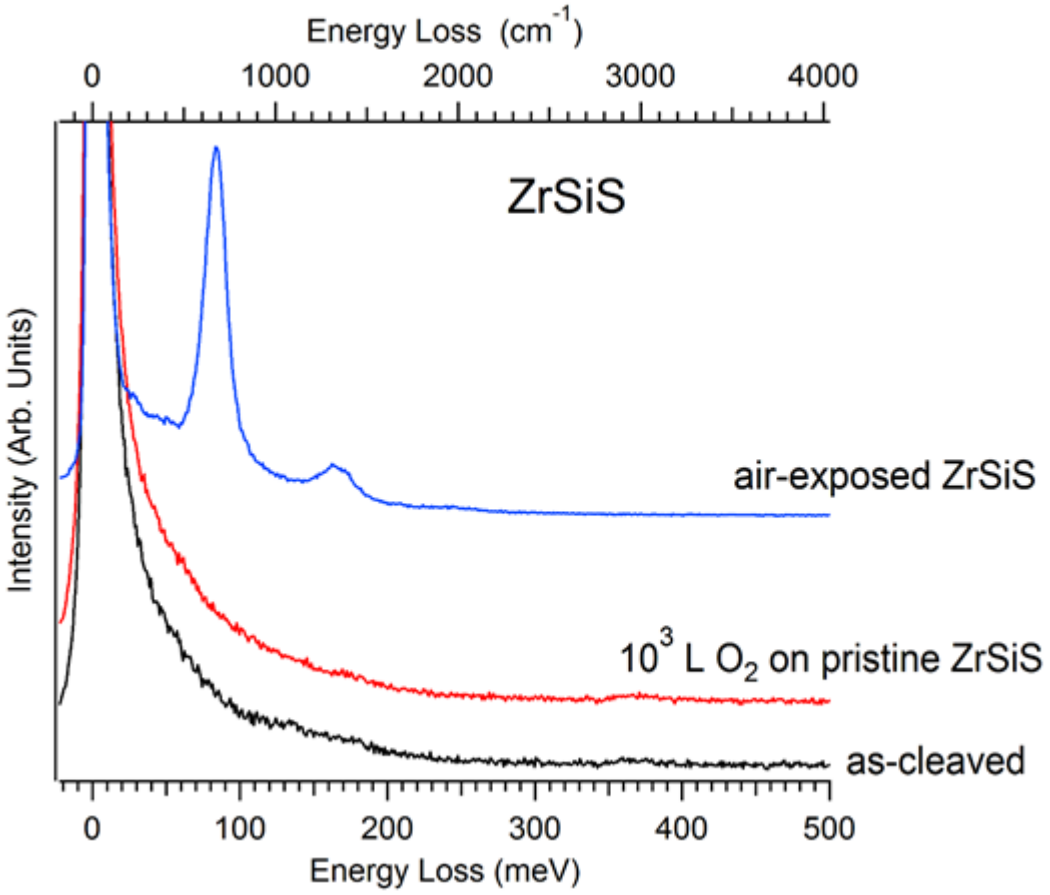

Figure 1: Vibrational spectra of pristine and modified ZrSiS systems. The black curve is related to as-cleaved ZrSiS, while the red and blue curves correspond to ZrSiS and $Zr_{1.05}Si_{0.98}S_{0.97}$ (defected ZrSiS) modified by the exposure to 10^3 L of O_2, respectively.

On the other hand, ZrSiSe has a much stronger reactivity toward oxygen. Specifically, the vibrational spectrum of O_2-dosed ZrSiSe has peaks at 56, 102 and 135 meV. The first mode should be associated to rocking Si-O-Si modes[37], while the remaining two to symmetric and anti-symmetric stretching ν_{sym}(Si–O)[38] and ν_{asym}(Si–O)[38] vibrations. Remarkably, the vibrational spectrum does not change significantly upon air exposure, thus indicating that surface passivation occurs already for 20 L of O_2.

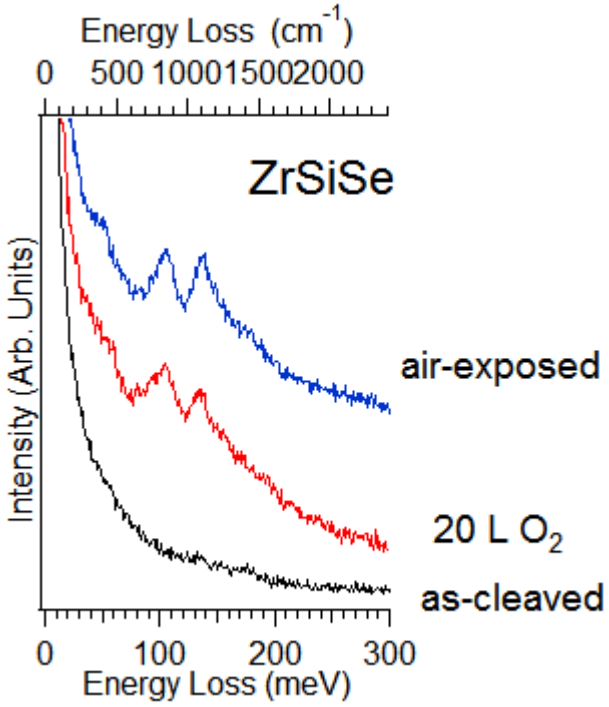

Figure 2: Vibrational spectra of pristine and modified ZrSiSe systems. The black curve is related to as-cleaved ZrSiSe, while the red and blue curves correspond to ZrSiS exposed to 20 L of O_2 and to air, respectively.

To gain a deeper insight on surface chemical bonds, the analysis of the core levels measured by X-ray photoelectron spectroscopy (XPS) represents an ideal complement to vibrational investigations. The core-level spectrum of as-cleaved ZrSiSe surface shows features at a binding energy (BE) of 182.8, 180.4, 166.8, 160.1 and 150.8 eV, attributed to Zr-$3d_{3/2}$, Zr-$3d_{5/2}$, Se-$3p_{1/2}$, Se-$3p_{3/2}$ and Si-2s core levels. The exposure to O_2 induces the emergence of shoulders for Si-2s and Zr-3d core levels. Especially, the component at 154.2 eV for Si-2s is typical of SiO_2 [39, 40], as also confirmed by the analysis of Si-2p core levels (SI, Figure S3). The spectral weight of components due to oxidation increases upon air exposure. Similarly, air exposure induces oxidation of Zr and Si adsorption sites in ZrSiS, while O_2 exposure does not induce significant changes in core levels, even if from survey XPS spectra we can estimate

the saturation oxygen coverage to be 0.15±0.02 ML and 1.58±0.05 ML for O_2-dosed ZrSiS and ZrSiSe, respectively. Correspondingly, by means of quantitative XPS analysis we estimate for ZrSiS (ZrSiSe) an oxide thickness of 0.4 Å (4.6 Å) and 6.4 Å (6.9 Å) after O_2 dosage and air exposure, respectively.

A careful inspection of Zr-3d core levels of the O_2-dosed ZrSiS surface reveals the appearance of a satellite for a BE of 185 eV, previously observed in the early stages of oxidation of Zr surfaces [41].

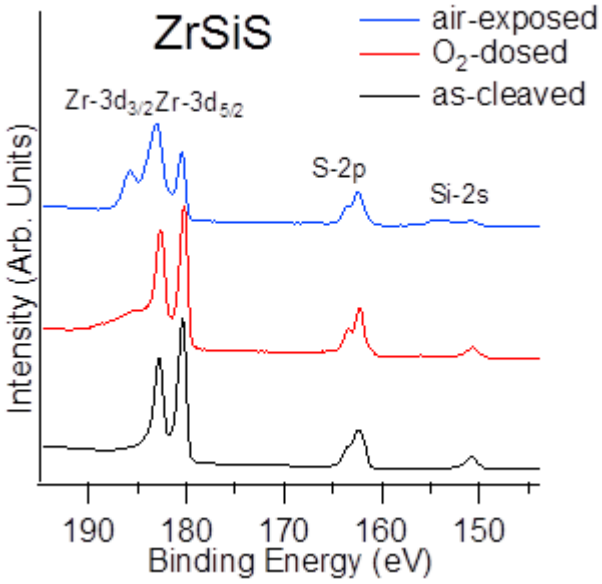

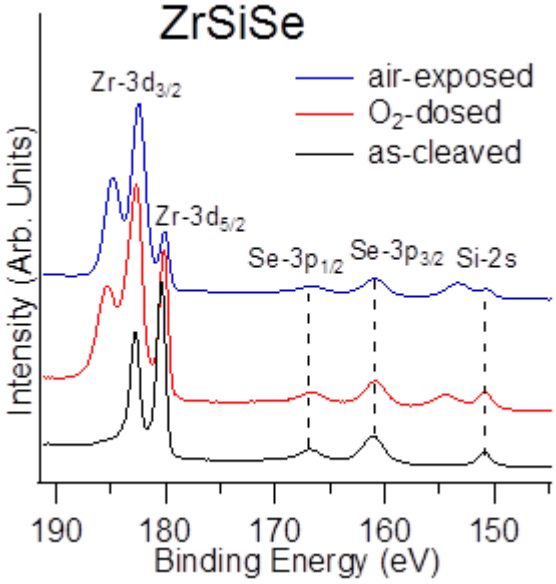

Figure 3. Core-level spectra for ZrSiS and ZrSiSe. Black, red, and blue curves correspond to as-cleaved, O_2-dosed and air-exposed samples, respectively. The photon energy is 800 eV.

To achieve a detailed comprehension on the surface chemical reactivity of ZrSiX systems, we have built a theoretical model of the adsorption process of reactants. The supercell has been modelled as described in the Methods, obtaining a good agreement between XRD experiments and theory concerning the value of the c-parameter of the ZrSiX crystals (Tab. 1). The modelling of Zr- and Si-terminated surfaces requires different slabs (see Figs. 4 and 5). In the case of Zr-terminated surfaces, no dangling bonds on the surface exist. Conversely, surfaces terminating with Si (Fig. 5e-h) have dangling bonds.

Firstly, we evaluate the energetics of the physical adsorption of single oxygen molecule on Zr (Fig. 4a and 5a) or Si (Fig. 5e) sites. In the case of Zr sites, adsorption is energetically favorable for all ZrSiX systems (see the column associated to step I in Tab. I). Correspondingly, strong Zr-O_2 bonds are formed (see Fig. 4a and 5a), whose strength is caused by the overlap between empty 4d orbitals of Zr^{4+} and lone pairs on 2p orbitals of oxygen.

In the case of Si sites, physical adsorption of molecular oxygen is energetically favorable only for the case of ZrSiSe. In the case of ZrSiTe, this process is extremely unfavorable, while for ZrSiS the energy of physisorption is almost zero, resulting in an unstable adsorption. The origin of this difference stands in the strong distortion of the ZrX layer under the silicon top layer. We define the thickness of the ZrX layer as the difference between projections of the nearest Zr and X atoms on the c-axis. In the case of ZrSiS, the thickness is almost the same as in bulk (0.88 vs 0.91 Å). However, in the case of ZrSiSe surface the thickness increases from 1.25 (bulk value) to 1.51 Å with the formation of the surface and a similar value is obtained for ZrSiTe (1.44 Å). Correspondingly, the distance between the Zr-X layer and the Si-layer is

influenced too, being maximal for ZrSiSe (2.61 Å vs 2.33 Å for ZrSiS). Such a described swelling of the surface makes Si-sites of ZrSiSe extremely chemically active. These seemingly small distortions of the lattice are crucial for the realization of the tetrahedral coordination of sp^3-hydridized silicon ions as in bulk ZrSiX, where Si is connected by three covalent bonds with Zr and by one bond with another Si atom in the same layer. The increase of the ZrX-Si interlayer distance facilitates the formation of the tetrahedral environment after adsorption of oxygen and makes S-terminated surface less stable.

After physical adsorption of the first oxygen molecule, two scenarios could be realized. The first possible process is the further adsorption of oxygen molecules on all active sites of the surfaces (Figs. 4b, 5b and 5f). In the case of Zr sites of ZrSiTe, which is energetically unfavorable (see column related to step II in Tab. I). An alternative scenario is represented by the decomposition of single physisorbed molecule (Fig. 4c, 5c and 5g). For the case of the Zr-terminated surface, this process is energetically favorable for all studied systems. Thus, we can conclude that, for the Zr-terminated surface of all studied systems, adsorbed oxygen molecules are decomposed. In the case of Si-terminated surface, formation of the molecular oxygen layer (Fig. 4b, 5b and 5f) is energetically favorable only for ZrSiSe. However, the decomposition of oxygen molecules is much more favorable than the formation of an O_2 layer. Thus, for all systems and all surfaces, physical adsorption of O_2 molecules is followed by their decomposition in O atoms.

As a final step of our model, we also evaluate the energetics of further decomposition of oxygen molecules on the surfaces until the oxidation of all suitable sites (Figs. 4d, 5d, 5h). Results of the calculations (see column related to step IV in Tab. I) demonstrate that this process is energetically favorable for both surfaces of all studied systems. Therefore, we can conclude that oxygen adsorption and decomposition with further oxidation of whole surface occur for

Zr sites of all studied system and for Si sites of only ZrSiSe. These results are evidently in qualitative agreement with experimental results (Figs. 1-3).

It is worth pointing out that two well-distinct scenarios concerning the reconstruction of Zr-terminated surface are feasible. The first scenario corresponds with the formation of dangling bonds between O and Zr atoms. In this case, Zr^{4+} ions form two additional bonds with X atom from the same layer, with the subsequent breaking of Zr-X bonds with the sublayer and the resulting decoupling of ZrOX layer (Fig. 4d). Another scenario is related to the formation of O bridges between two Zr atoms on the surface (Fig. 5d). The predominance of one or another scenario of the reconstruction of Zr-terminated surface depends on the specific ZrSiX compound and it is directly associated to the different distortions and interlayer distances. The strong distortions of the surface layers and the possibility of the detachment of surface layers makes the use of ZrSiX as catalysts rather problematic, since poisoning of the catalyst seems unavoidable. In ZrSiSe, larger distances between the atoms occur (especially between the layers), with a resulting smaller structural stability and, consistently, higher chemical activity. Figs. 5e-h demonstrate how the interaction of Si-sites with the oxygen provides delamination of layers of ZrSiSe. This decoupling of the layers affords limits for the oxidation process and, correspondingly, the surface oxide phase will have a maximum thickness of a few Å.

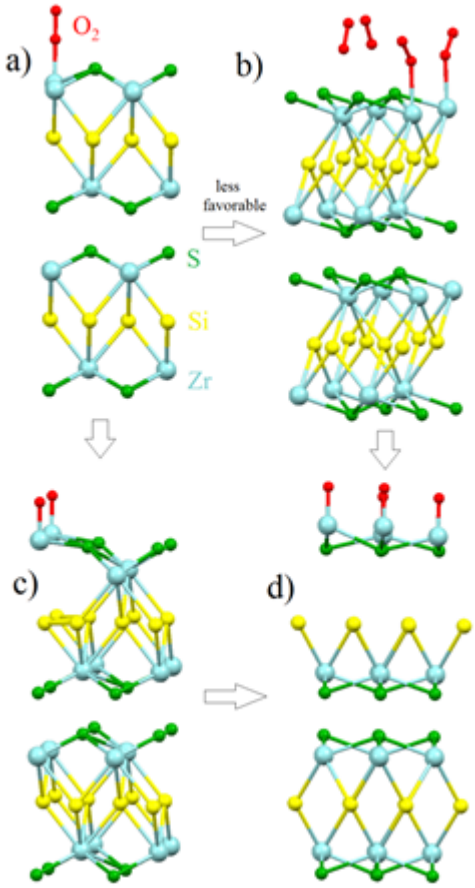

Figure 4. Optimized atomic structure of different steps of the process of the oxidation of ZrSiS from Zr-sites. Red, light blue, green and yellow balls represent O, Zr, S, and Si atoms, respectively. The various panels depict: (a) physical adsorption of a single oxygen molecule; (b) uniform coverage of the surface by molecular oxygen; (c) decomposition of single oxygen molecule on the surface and (d) total oxidation of the surface.

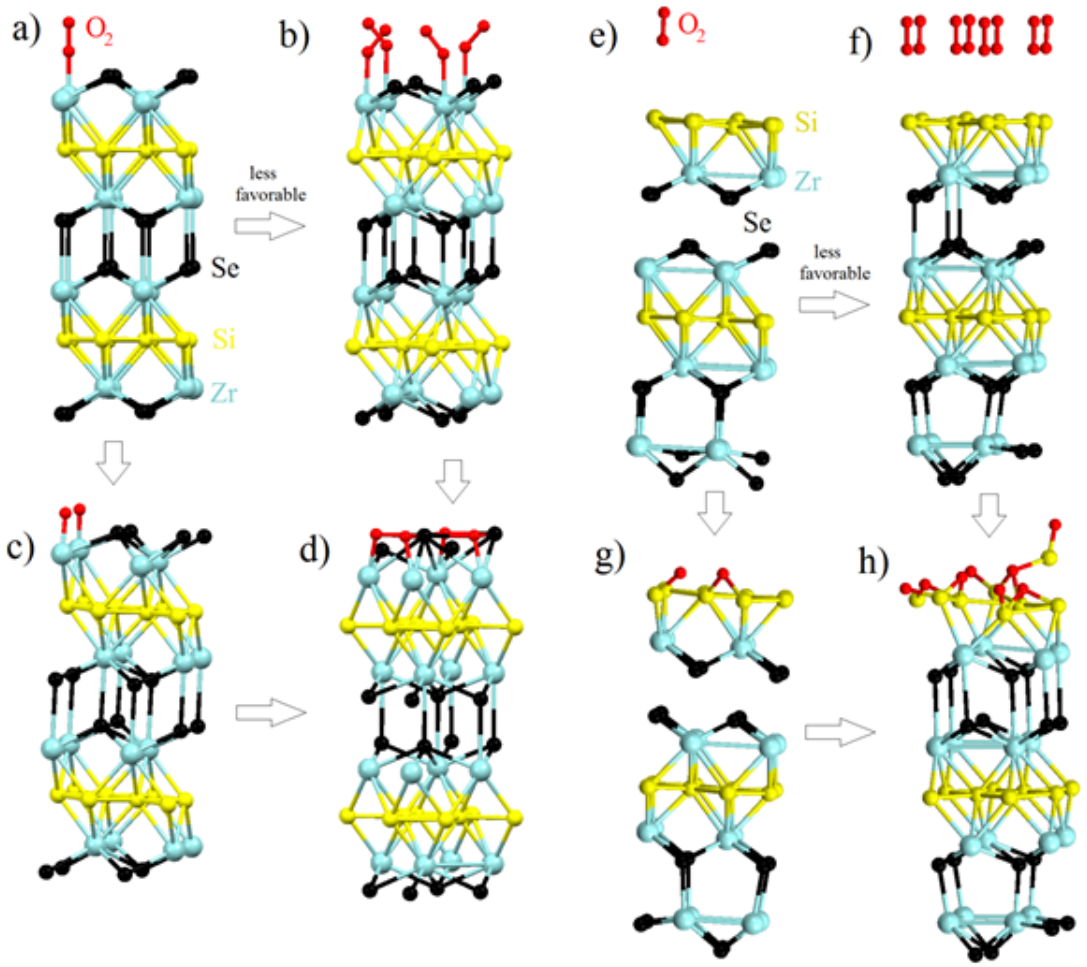

Figure 5. Atomic structure of different steps of the process of the oxidation of ZrSiSe from (a-d) Zr-sites and (e-h) Si-sites. Red, light blue, black and yellow balls represent O, Zr, Se, and Si atoms, respectively. On panels (a) and (e) physical adsorption of single oxygen molecule is depicted. Panels (b) and (f) represent the situation of uniform coverage of the surfaces by molecular oxygen. In panels (c) and (g), decomposition of single oxygen molecule on the surfaces is represented. Panels (d) and (h) show total oxidation of the surfaces.

Table I. Activation energies for the formation of ZrSiX surfaces (E_{form}) and for their oxidation depending on their respective termination. Lattice parameters are also reported. Steps of the oxidation process correspond with those depicted in Figs. 4 and 5. The first energetically unfavorable steps, corresponding to the termination of the oxidation process, are marked by bold.

E_{form} (eV)	a (Å)	c (Å)	Termination	Oxidation step (eV/O_2)			
				I	II	III	IV
ZrSiS (+1.36)	3.506	8.327	Zr	-0.64	-0.66	-1.31	-0.41
			Si	-0.03	**+2.39**	-7.22	-0.62
ZrSiSe (+1.45)	3.576	8.827	Zr	-0.76	-0.63	-0.44	-2.08
			Si	-5.60	-0.65	-7.75	-6.37
ZrSiTe (+1.57)	3.675	10.344	Zr	-2.76	**+2.41**	+0.64	-1.42
			Si	**+5.41**	+0.82	-7.80	-5.32

Another important issue is to unveil how surface oxidation modifies the electronic structure of ZrSiX compounds. The density of states (DOS) calculated for bulk ZrSiX (Fig. 6a) is evidently semimetal-like, corresponding with topological features in band structure typical of NLSM (Fig. 7a,b). After the formation of the most favorable Zr-terminated surface, peaks in the DOS arising from 4d bands of surface Zr atoms appear near the Fermi level (Fig. 6c). Congruently, these features also observed in experimental valence-band spectra of as-cleaved samples (Fig. 8). Remarkably, the formation of the surface implies the withdrawal of all topological features of the bulk in the surface band structure (Figs. 7c,d). Note that the DOS corresponding to the case of less energetically favorable Si-terminated surface, reported in Fig.

S4, is significantly different from experimental valence-band spectra in Fig. 8. Thus, we can conclude that samples have a predominant Zr-terminated surface and, consistently, Si-terminated surface is rare. Both experiment and theory for as-cleaved surfaces show broadened electronic bands, with the survival of a well-distinct peak at 2 eV of BE (Figs. 7c,d and 8), originated by bulk Zr-4d states (Fig. 7a,b). Experimental spectra also indicate a notable difference in electronic structure of oxidized surfaces compared to pristine ones. In the case of ZrSiSe, we observed the disappearance of the peaks near Fermi level in contrast to oxidized ZrSiS, where some states at the Fermi level are observed. Calculations also demonstrate vanishing of the peak below Fermi level in ZrSiSe and the appearance of the peak around the Fermi level in oxidized ZrSiS slab. Such differences are originated by the dissimilar atomic structure of oxidized surfaces. Specifically, for oxidized surface of ZrSiSe we observe formation of rather uniform ZrSeO layer (Fig. 5d). In the case of ZrSiS, decoupling of ZrSO layer occurs. The formation of this decoupled layer provides breaking of covalent bonds between surface and subsurface layers and the appearance of the contribution from Si and S 3*p* bands around the Fermi level. The presence of the oxidized ZrXO surface layers induces appearance of additional features in the band structure although the surface band structure is generally maintained (Fig. 7e,f).

Both experimental and theoretical results suggest that it is crucial to protect the surfaces of ZrSiX materials. In contrast to the case of phosphorene [42] and other layered materials [43-45], an appropriate capping layer for ZrSiX should combine (i) the prevention of the interaction of the surface with oxidative species and (ii) the saturation of dangling bonds with minimal distortion of the surface. Particularly, we have explored the viability of passivation by hydrogenation finding complex phenomena described in details in the SI (Fig. S6 and its related discussion). Calculations demonstrate that hydrogenation eliminates bands at the Fermi level

corresponding with dangling bonds on the bare surface (Fig. S5c,d). Nevertheless, hydrogenation of the surfaces does not restore bulk-like band structure. On the other hand, hydrogenation induces the appearance of novel electronic states around the Fermi level. Thus, the functionalization of the surface of topological materials could be a tool not only for protecting the surface but also for engineering topologic electronic states.

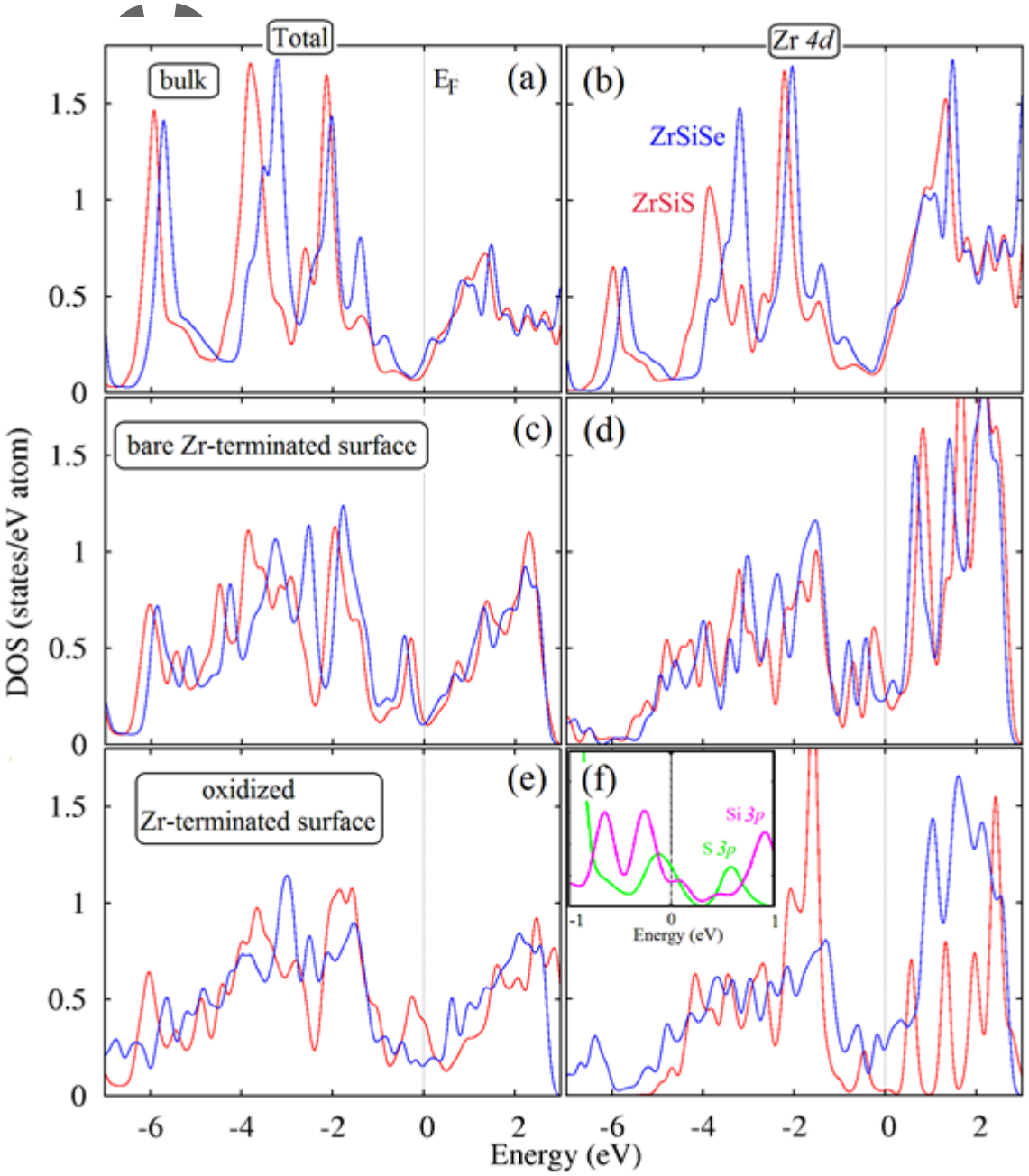

Figure 6. Total densities of states for (a) bulk and for a slab with (c) bare and (e) oxidized Zr-terminated surfaces of ZrSiS and ZrSiSe. We also report partial densities of Zr *4d* states from

(b) bulk and from (d) bare and (f) oxidized slabs corresponding to surface layers. In the inset to panel (f), we report partial densities of states for S *3p* from surface layer and Si *3p* from subsurface layer of oxidized slab of ZrSiS.

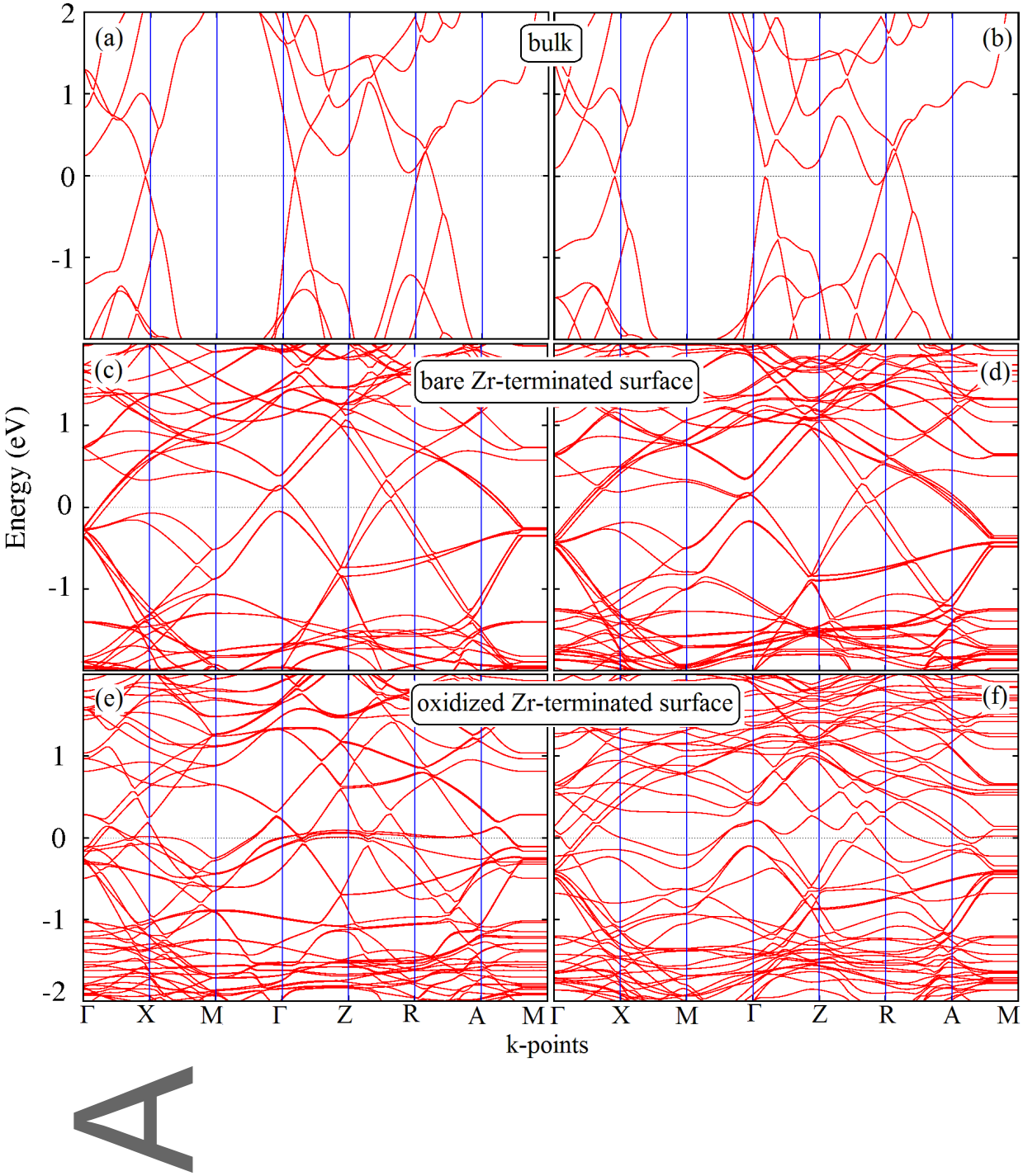

Figure 7. Band structure of bulk (a) ZrSiS and (b) ZrSiSe, the slab with Zr-terminated surface for (c) ZrSiS and (d) ZrSiSe, (e) ZrSiS slab oxidized from Zr-sites (see Fig. 4d), and (f) the ZrSiSe slab oxidized from Si-sites (Fig. 5h).

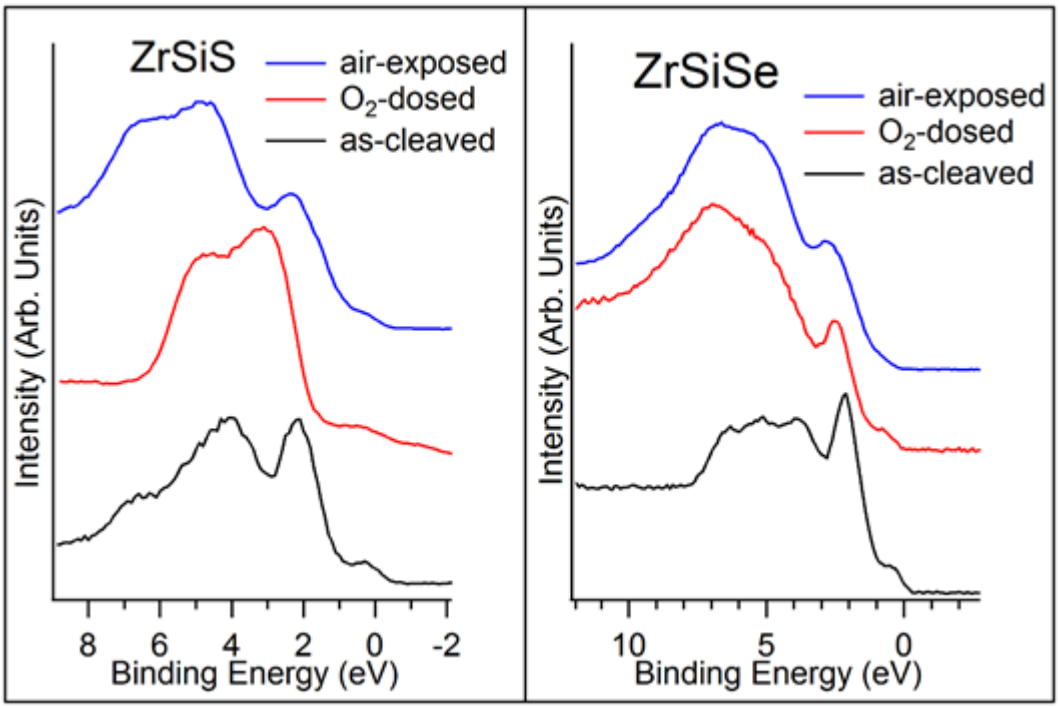

Figure 8. Valence-band spectra of ZrSiS and ZrSiSe. Black, red, and blue curves correspond to as-cleaved, O_2-dosed and air-exposed samples, respectively. The photon energy is 400 eV.

Conclusions

We have demonstrated that the chemical activity of ZrSiX compounds is mainly determined by the interactions of Si layer with ZrX sublayer. Any adsorption provides distortion of the Si layer (flat in bulk). In the case of ZrSiS, the ZrS sublayer is almost the same as in bulk and

therefore adsorption is unfavorable, because it provides distortions of Si-layer. In the case of ZrSiSe, the ZrSe sublayer is already strongly distorted (structure different from bulk) and, therefore, further distortion of Si-layer by adsorption is favorable. Hence, an appropriate encapsulation procedure should not only protect surfaces from oxidative species, but also saturate dangling bonds with minimal distortion of the surface.

Moreover, we have shown that the formation of the surface induces the disappearance of topological features typical of NLSM.

We can conclude that the relationship between surface chemical reactivity and NLSM has unique characteristics, which makes this class of topological materials particularly promising for applications exploiting the ultrahigh magnetoresistance and charge-carrier mobility.

Methods

Growth of single crystals

Single crystals of ZrSiS and ZrSiSe were grown using the chemical vapor transport method with I_2 as the transport agent. For ZrSiS, the polycrystalline precursor was first obtained from a stoichiometric mixture of Zr, Si, and S powder. The starting materials were sealed in an evacuated quartz tube, heated up to 1100 °*C* in a furnace and kept for one week, followed by furnace-cooled down to room temperature. The obtained polycrystalline ZrSiS was then mixed with I_2 in weight ratio of 100:1 and vacuum-sealed in a two-zone tube furnace having a thermal gradient of about 1100-950°*C* within ~30 cm. Single crystals of ZrSiS with size up to 4.0 × 2.9 × 3.0 mm^3 can be obtained after 10 days [28]. For ZrSiSe, the chemical vapor transport was performed directly using the stoichiometric mixture of Zr, Si, and Se

powder with I_2. Large crystals up to a half centimeter can be obtained with the temperature gradient of 950-850°*C* [22].

Surface-science investigations

Single crystals of ZrSiS and ZrSiSe were cleaved in ultrahigh vacuum (UHV) and their composition was controlled by means of Auger electron spectroscopy (AES) and XPS. Survey XPS spectra reported in Fig. S7 of the SI demonstrate the cleanliness of starting single-crystals.

XPS experiments were performed at the High-Energy branch of the Advanced Photoelectric Experiments beamline (APE-HE) of the Elettra Synchrotron, Trieste, Italy. XPS spectra were collected with an Omicron EA125 hemispherical electron energy analyzer, with the sample at room temperature and in normal emission condition. The linearly polarized light was impinging on the sample forming an angle of 45 degrees with respect to the normal to the surface. To evaluate binding energies of core levels, a Shirley background was subtracted from XPS spectra.

Vibrational experiments on surface chemical reactivity were performed by means of HREELS at University of Calabria, Italy. We used a Delta 0.5 spectrometer by SPECS GmbH, Germany with an energy resolution of about 3 meV. The primary electron beam energy E_p in vibrational investigations was 3 eV. All vibrational spectra were acquired with the sample kept at RT. To extract vibrational frequencies, an exponential background was subtracted from each HREELS spectrum. Defects have been implanted by low-energy ion sputtering (primary energy in the range 300-600 eV) for HREELS experiments at University of Calabria, Italy. Surface composition of defected samples has been checked by AES.

Air exposure has been carried out by exposing the sample in ambient atmosphere.

DFT calculations

The atomic structure and energetics of various configurations have been studied by DFT using the QUANTUM-ESPRESSO code [46] and the GGA–PBE + van der Waals (vdW) approximation, feasible for the description of the adsorption of molecules on surfaces [47, 48]. We used energy cutoffs of 25 Ry and 400 Ry for the plane-wave expansion of the wave functions and the charge density, respectively, and the 4×4×2 Monkhorst-Pack *k*-point grid for the Brillouin sampling. [49]

For the modeling of the surface of ZrSiX compounds, we used a slab constructed from 2×2×2 supercell. The separation between the layers is about 20 Å. Physisorption energies were calculated by the standard formula:

$$\Delta E_{phys} = [E_{host+mol} - (E_{host} + E_{mol})],$$

where E_{host} is the total energy of pure surface, and E_{mol} is the energy of the single molecules of selected species in empty box.

Chemisorption energy is defined as difference between the total energy of the system with physically adsorbed molecule (Fig. 4a) and the total energy of same system after decomposition of the same molecule on the surface (Fig. 4b).

As we study the processes at room temperature, the contribution from the entropy ($T\Delta S$) in Gibbs free energy should be taken into account. For the physical adsorption of the oxygen we estimated this value by the entropy gas to liquid transition by standard formula:

$$\Delta S = \Delta H_{vaporisation}/T,$$

where $\Delta H_{vaporization}$ is the measured enthalpy of vaporization and T is the corresponding temperature. Obtained value of TΔS for molecular oxygen is 0.117 eV. For the estimation of the entropy of decomposition of the oxygen on open Zr-site, we compare the change of the entropy in the transition from α-Zr to ZrO_2. [49, 50] At room temperature, TΔS contribution to the Gibbs free energy of oxygen decomposition is 0.017 eV. As the magnitude of both these values is much smaller than the magnitudes of the energies of formation, we will further consider only the contribution from differential enthalpy (see Tab. I).

Acknowledgments

AP thanks Elettra Sincrotrone Trieste S.C.p.A. for financial support. ZM thanks the support by the US Department of Energy under grant DE-SC0014208 for material synthesis. This work has been partly performed in the framework of the nanoscience foundry and fine analysis facility (NFFA-MIUR Italy Progetti Internazionali).

Conflict of Interest
The authors declare no conflict of interest.

Keywords
density functional theory, surface science, topological materials, vibrational spectroscopy, X-ray photoelectron spectroscopy

References

[1] F. D. M. Haldane, Rev. Mod. Phys. **2017**, 89, 040502.
[2] F. Wang, L. Li, W. Huang, L. Li, B. Jin, H. Li, T. Zhai, Adv. Funct. Mater. **2018**, 28, 1802707.
[3] P. Tsipas, S. Fragkos, D. Tsoutsou, C. Alvarez, R. Sant, G. Renaud, H. Okuno, A. Dimoulas, Adv. Funct. Mater. **2018**, 28, 1802084.
[4] S. Ma, C. Guo, C. Xiao, F. Wu, M. Smidman, Y. Lu, H. Yuan, H. Wu, Adv. Funct. Mater. **2018**, 28, 1803188.
[5] S. Hao, J. Zeng, T. Xu, X. Cong, C. Wang, C. Wu, Y. Wang, X. Liu, T. Cao, G. Su, L. Jia, Z. Wu, Q. Lin, L. Zhang, S. Yan, M. Guo, Z. Wang, P. Tan, L. Sun, Z. Ni, S. J. Liang, X. Cui, F. Miao, Adv. Funct. Mater. **2018**, 28, 1803746.
[6] A. Thakur, K. Sadhukhan, A. Agarwal, Phys. Rev. B **2018**, 97, 035403.
[7] K. Das, A. Agarwal, Phys. Rev. B **2019**, 99, 085405.
[8] H. Huang, K. H. Jin, F. Liu, Phys. Rev. Lett. **2018**, 120, 136403.
[9] B. Singh, B. Ghosh, C. Su, H. Lin, A. Agarwal, A. Bansil, Phys. Rev. Lett. **2018**, 121, 226401.
[10] B. Singh, S. Mardanya, C. Su, H. Lin, A. Agarwal, A. Bansil, Phys. Rev. B **2018**, 98, 085122.
[11] J. Wu, Y. Lu, S. Feng, Z. Wu, S. Lin, Z. Hao, T. Yao, X. Li, H. Zhu, S. Lin, Adv. Funct. Mater. **2018**, 28, 1804712.
[12] A. F. Carvalho, A. J. S. Fernandes, C. Leitão, J. Deuermeier, A. C. Marques, R. Martins, E. Fortunato, F. M. Costa, Adv. Funct. Mater. **2018**, 28, 1805271.

[13] H. A. Hafez, S. Kovalev, J. C. Deinert, Z. Mics, B. Green, N. Awari, M. Chen, S. Germanskiy, U. Lehnert, J. Teichert, Z. Wang, K. J. Tielrooij, Z. Liu, Z. Chen, A. Narita, K. Müllen, M. Bonn, M. Gensch, D. Turchinovich, Nature **2018**, 561, 507.
[14] D. Maccariello, A. Al Taleb, F. Calleja, A. L. Vázquez de Parga, P. Perna, J. Camarero, E. Gnecco, D. Farías, R. Miranda, Nano Lett. **2016**, 16, 2.
[15] B. Feng, O. Sugino, R.-Y. Liu, J. Zhang, R. Yukawa, M. Kawamura, T. Iimori, H. Kim, Y. Hasegawa, H. Li, L. Chen, K. Wu, H. Kumigashira, F. Komori, T.-C. Chiang, S. Meng, I. Matsuda, Phys. Rev. Lett. **2017**, 118, 096401.
[16] D. Li, J. He, G. Ding, Q. Tang, Y. Ying, J. He, C. Zhong, Y. Liu, C. Feng, Q. Sun, H. Zhou, P. Zhou, G. Zhang, Adv. Funct. Mater. **2018**, 28, 1801685.
[17] X. Sun, X. Liu, J. Yin, J. Yu, Y. Li, Y. Hang, X. Zhou, M. Yu, J. Li, G. Tai, W. Guo, Adv. Funct. Mater. **2017**, 27, 1603300.
[18] K. Sadhukhan, A. Agarwal, Phys. Rev. B **2017**, 96, 035410.
[19] C. Li, C. Wang, B. Wan, X. Wan, H.-Z. Lu, X. Xie, Phys. Rev. Lett. **2018**, 120, 146602.
[20] R. A. Molina, J. González, Phys. Rev. Lett. **2018**, 120, 146601.
[21] C. Li, C. M. Wang, B. Wan, X. Wan, H. Z. Lu, X. C. Xie, Phys. Rev. Lett. **2018**, 120, 146602.
[22] J. Hu, Z. Tang, J. Liu, X. Liu, Y. Zhu, D. Graf, K. Myhro, S. Tran, C. N. Lau, J. Wei, Z. Mao, Phys. Rev. Lett. **2016**, 117, 016602.
[23] S. Pezzini, M. R. Van Delft, L. M. Schoop, B. V. Lotsch, A. Carrington, M. I. Katsnelson, N. E. Hussey, S. Wiedmann, Nat. Phys. **2018**, 14, 178.
[24] M. S. Lodge, G. Chang, C. Y. Huang, B. Singh, J. Hellerstedt, M. T. Edmonds, D. Kaczorowski, M. M. Hosen, M. Neupane, H. Lin, M. S. Fuhrer, B. Weber, M. Ishigami, Nano Lett. **2017**, 17, 7213.
[25] A. N. Rudenko, E. A. Stepanov, A. I. Lichtenstein, M. I. Katsnelson, Phys. Rev. Lett. **2018**, 120, 216401.
[26] C. Wang, T. Hughbanks, Inorg. Chem. **1995**, 34, 5524.
[27] R. Singha, A. K. Pariari, B. Satpati, P. Mandal, Proc. Natl. Acad. Sci. U. S. A. **2017**, 114, 2468.
[28] R. Sankar, G. Peramaiyan, I. P. Muthuselvam, C. J. Butler, K. Dimitri, M. Neupane, G. N. Rao, M. T. Lin, F. C. Chou, Sci. Rep. **2017**, 7, 40603.
[29] L. M. Schoop, M. N. Ali, C. Strasser, A. Topp, A. Varykhalov, D. Marchenko, V. Duppel, S. S. Parkin, B. V. Lotsch, C. R. Ast, Nat. Commun. **2016**, 7, 11696.
[30] M. Matusiak, J. R. Cooper, D. Kaczorowski, Nat. Commun. **2017**, 8, 15219.
[31] M. N. Ali, L. M. Schoop, C. Garg, J. M. Lippmann, E. Lara, B. Lotsch, S. S. P. Parkin, Science Advances **2016**, 2, e1601742.
[32] X. He, W. Zhou, Z. Y. Wang, Y. N. Zhang, J. Shi, R. Q. Wu, J. A. Yarmoff, Phys. Rev. Lett. **2013**, 110, 156101.
[33] A. Politano, G. Chiarello, Z. Li, V. Fabio, L. Wang, L. Guo, X. Chen, D. W. Boukhvalov, Adv. Funct. Mater. **2018**, 28, 1800511.
[34] H. Ibach, D. L. Mills, *Electron Energy Loss Spectroscopy and Surface Vibrations*, Academic Press, San Francisco 1982.
[35] R. Fuchs, K. L. Kliewer, Phys. Rev. **1965**, 140, A2076.
[36] P. A. Dilara, J. M. Vohs, J. Phys. Chem. **1993**, 97, 12919.
[37] G. Lucovsky, G. Rayner Jr, Appl. Phys. Lett. **2000**, 77, 2912.
[38] L. Giordano, D. Ricci, G. Pacchioni, P. Ugliengo, Surf. Sci. **2005**, 584, 225.
[39] S. Sareen, V. Mutreja, B. Pal, S. Singh, Appl. Surf. Sci. **2018**, 435, 552.
[40] N. Kawada, M. Ito, Y. Saito, Jpn. J. Appl. Phys. **2006**, 45, 9197.
[41] C. Morant, J. M. Sanz, L. Galán, L. Soriano, F. Rueda, Surf. Sci. **1989**, 218, 331.
[42] J. O. Island, G. A. Steele, H. S. J. van der Zant, A. Castellanos-Gomez, 2D Mater. **2015**, 2, 011002.
[43] S. A. Wells, A. Henning, J. T. Gish, V. K. Sangwan, L. J. Lauhon, M. C. Hersam, Nano Lett. **2018**, 18, 7876.

[44] Q. Zhao, R. Frisenda, P. Gant, D. Perez de Lara, C. Munuera, M. Garcia-Hernandez, Y. Niu, T. Wang, W. Jie, A. Castellanos-Gomez, Adv. Funct. Mater. **2018**, 28, 1805304.
[45] S. Yang, H. Cai, B. Chen, C. Ko, V. O. Ozcelik, D. F. Ogletree, C. E. White, Y. Shen, S. Tongay, Nanoscale **2017**, 9, 12288.
[46] P. Giannozzi, S. Baroni, N. Bonini, M. Calandra, R. Car, C. Cavazzoni, D. Ceresoli, G. L. Chiarotti, M. Cococcioni, I. Dabo, A. Dal Corso, S. de Gironcoli, S. Fabris, G. Fratesi, R. Gebauer, U. Gerstmann, C. Gougoussis, A. Kokalj, L. Michele, L. Martin-Samos, N. Marzari, F. Mauri, R. Mazzarello, S. Paolini, A. Pasquarello, L. Paulatto, C. Sbraccia, S. Scandolo, G. Sclauzero, A. P. Seitsonen, A. Smogunov, P. Umari, R. M. Wentzcovitch, J. Phys.: Condens. Matter **2009**, 21, 395502.
[47] J. P. Perdew, K. Burke, M. Ernzerhof, Phys. Rev. Lett. **1996**, 77, 3865.
[48] V. Barone, M. Casarin, D. Forrer, M. Pavone, M. Sambi, A. Vittadini, J. Comput. Chem. **2009**, 30, 934.
[49] H. J. Monkhorst, J. D. Pack, Phys. Rev. B **1976**, 13, 5188.
[50] S. Todd, J. Am. Chem. Soc. **1950**, 72, 2914.

Table of Content

The chemical activity of ZrSiX compounds is mostly determined by the interaction of Si layer with the ZrX sublayer.

A suitable encapsulation for ZrSiX should not only preserve their surfaces from interaction with oxidative species, but also provide a saturation of dangling bonds with minimal distortion of the surface.